

Pulsed inductive microwave magnetometer

Anthony B. Kos,^{a)} Thomas J. Silva, and Pavel Kabos
National Institute of Standards and Technology, Boulder, Colorado 80305

(Received 13 February 2002; accepted for publication 19 June 2002)

We describe the apparatus, software, and measurement procedures for a pulsed inductive microwave magnetometer (PIMM). PIMM can measure the dynamical properties of materials used in recording heads for magnetic storage applications, and it can be used as a general magnetodynamics diagnostic tool. PIMM uses a coplanar waveguide as both a source of fast pulsed magnetic fields and as an inductive flux sensor. Magnetic field pulses are provided by a 10 V, 55 ps risetime pulse generator; a 20 GHz digital sampling oscilloscope is used to acquire the fast pulse data; and orthogonal Helmholtz pairs provide the bias and saturating fields required for the measurement. The system can measure dynamical behavior as a function of several variables, including applied magnetic bias field, magnetic pulsed field amplitude and width, and sample orientation. Using a fast Fourier transform, PIMM can determine the frequency dependence of the complex magnetic permeability, as well as the step and impulse responses of the magnetic system. Data from 50 nm Ni-Fe and rare-earth-doped Ni-Fe thin films are presented. [DOI: 10.1063/1.1505657]

I. INTRODUCTION

As disk drive areal storage densities increase, there is an associated need for an increase in the rate with which the data can be transferred.¹ Advances in drive track-following servosystems, high-density media, giant magnetoresistive heads, and ultralow flying height sliders have led to large storage density increases, with disks carrying as much as 30 gigabytes (GBytes) on a single 8.9 cm (3.5 in.) platter.² Improvements in magnetic storage capacity are achieved through increased track and linear bit densities. These increases, when combined with high rotational speed spindle motors (15 000 rpm motors are currently available in advanced drives), lead to media data transfer rates in commercially available drives in excess of 650×10^6 bits per second.³ Clearly, the head materials used in these drives must respond magnetically at rates close to 1 GHz, and further increases in response rate will soon be required to keep up with the 60% annual growth rate seen in disk drive areal densities. Understanding the mechanisms involved in the dynamical processes of these materials is crucial for the development and design of read/write heads used in future magnetic data storage applications. For this purpose, we developed a pulsed inductive microwave magnetometer (PIMM).^{4,5} Inductive techniques to study high-speed thin-film dynamics were first developed in the 1960's by Smith⁶ and Wolf.⁷ Hiebert *et al.*⁸ also used pulsed fields but instead sensed the response using magneto-optical Kerr microscopy. More recently, Bauer *et al.*⁹ measured pulse-induced magnetic precession as a function of pulse width in order to optimize field pulse parameters in magnetic storage devices.

This article describes the apparatus, software, and procedures used to acquire data using the PIMM system. High-speed measurements of magnetization dynamics in 50 nm thick Ni-Fe ($\text{Ni}_{81}\text{Fe}_{19}$) thin films are shown. Generally,

Ni-Fe samples show a fast, slightly underdamped response to the fast magnetic pulse, a useful response for read/write head applications. In addition, we measured Tb-doped Ni-Fe samples with a magnetic response that included underdamped, critically damped, and overdamped characteristics.¹⁰ These samples show that the PIMM system is sensitive enough to measure even slowly changing inductive signals.

The PIMM system can measure dynamical magnetic behavior as a function of applied magnetic bias field, pulsed field amplitude, and pulsed field duration. The response, when measured in both hard and easy axes, can show both linear and nonlinear behavior. Using fast Fourier transform (FFT) analysis of step-response data, we can obtain the complex magnetic permeability as a function of frequency. In addition, we can automatically measure the impulse response (in time and frequency domains) of the magnetic films. The system has measured soft ferromagnetic materials such as Ni-Fe alloys,¹⁰ Co-Fe-Hf-O,¹¹ and Co-Zr-Ta. It has also been used to measure patterned films.¹²

The PIMM system uses a coplanar waveguide to deliver short risetime pulses to the film, which is placed film-side down onto the waveguide. A thin layer of photoresist is spun coated onto the film to prevent it from shorting to the waveguide. The coplanar waveguide also acts as the magnetic flux sensor, inductively coupling to the external magnetic flux generated by the sample when it switches. A fast pulse generator provides drive pulses with risetimes of 50 ps to the waveguide. The transmitted pulse, with the inductive response, is measured with a 20 GHz digital sampling oscilloscope. Impulse response measurements are accomplished by automatically switching in a two-port, passive, impulse-forming network between the pulse generator and the coplanar waveguide. Two orthogonal magnetic field sources pro-

^{a)}Electronic mail: kos@boulder.nist.gov

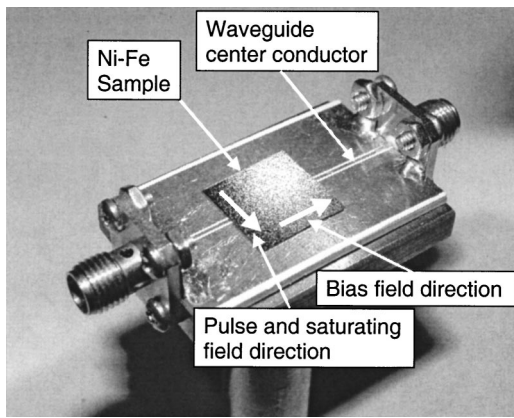


FIG. 1. Photograph of coplanar waveguide used in the PIMM system. A sample is seen face down and centered on the surface. Longitudinal bias (stiffening) fields are applied parallel to the center conductor, and transverse saturating fields, as well as the fast pulse generated by the waveguide, are applied perpendicular to this direction.

vide the bias and saturating fields necessary for the measurement. The entire system is computer controlled and hundreds of measurements can be made on a specimen in minutes without user intervention.

II. SAMPLES

Ni-Fe ($\text{Ni}_{81}\text{Fe}_{19}$) films, 50 nm thick, were grown by dc magnetron sputtering in the presence of a 16 kA/m (200 Oe) magnetic field onto glass cover slides, 18 mm \times 18 mm in size. In addition, Tb-doped Ni-Fe samples with doping levels of 0%, 2%, and 4% Tb were similarly prepared by cosputtering Ni-Fe and Tb at different Ar pressures and sputtering levels.¹⁰ These films were 50 nm thick, 1.0 cm \times 1.0 cm in size. Finally, a series of Ni-Fe films of varying thickness, from 10 to 500 nm in a 1-2-5 sequence, were fabricated as above, onto 18 mm \times 18 mm glass cover slides; however, the films over 200 nm thick had stress-induced disorder and had to be annealed at 350 °C for 1 h in order to induce a preferred anisotropy axis. A thin coating (less than 1 μm) of polyimide photoresist was spun onto all the films to

protect them and to prevent the films from shorting to the waveguide conductors. The films were then measured on a conventional induction-field ($B-H$) loop to determine their magnetic properties, such as coercivity and anisotropy, which are useful to know before measuring with the PIMM.

III. APPARATUS

The coplanar waveguide used as both a pulsed field source and an inductive sensor is constructed using standard lithographic techniques. It is shown along with a Ni-Fe sample in Fig. 1. The material used for the waveguide is double-sided, copper-clad duroid board, 1.27 mm (0.050 in.) thick with 0.025 mm (0.001 in.) thick copper cladding; the relative permittivity of the dielectric is 10.2. The waveguide center conductor is 500 μm wide and the spacing between the center conductor and the 10 mm wide ground planes is 225 μm . The duroid board material used to construct the waveguide is soft and not very useful as a structural material, so the waveguide board is permanently mounted onto a 36 mm \times 25 mm (1.4 in. \times 1.0 in.) brass base plate that is drilled and tapped to accept standard optical posts. To make contact to the waveguide, two standard subminiature A (SMA) flange mount connectors are rigidly fixed to the brass base plate and electrically connected to the ground planes of the waveguide by means of copper shims soldered to the ground planes and bolted to the SMA connectors. The 0.51 mm (0.020 in.) center tab of the SMA flange mount is connected to the center conductor of the waveguide by pressure contact only (no solder is used); this produces a connection with low voltage standing wave ratio and high bandwidth, and allows convenient disassembly of the waveguide. The nominal characteristic impedance, determined by time-domain reflectometry, of the completed waveguide is 50 ± 0.5 ohm and the bandwidth, as determined by step rise-time, is greater than 10 GHz. Square samples up to 25 mm \times 25 mm (1.0 in. \times 1.0 in.) can be accommodated.

A schematic of the overall system is shown in Fig. 2. The ultrafast pulse generator used produces 10 V, 55 ps rise-time pulses and has full computer control of pulse width,

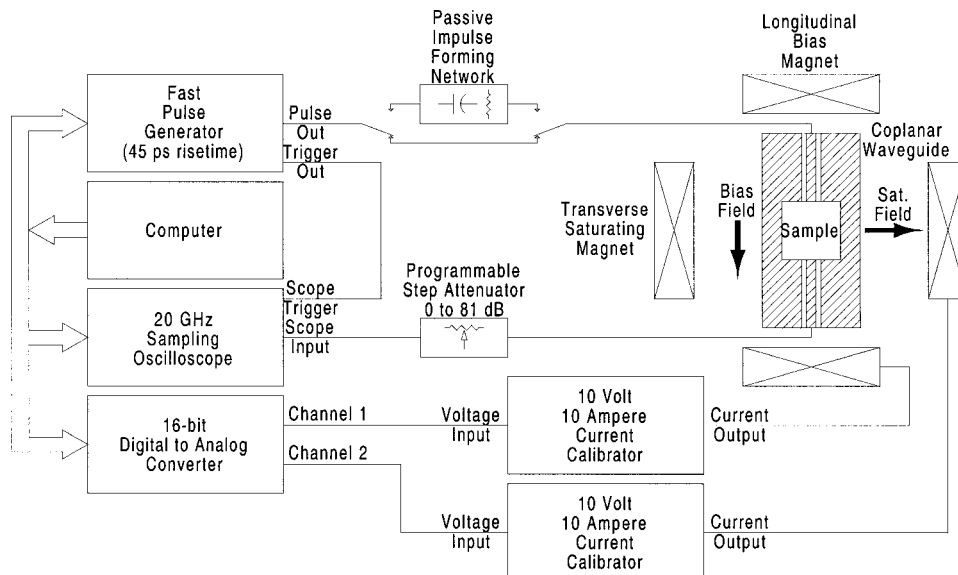


FIG. 2. Schematic diagram of the PIMM system showing fast pulse generator with impulse-forming network, sampling scope with high-bandwidth attenuators, computerized orthogonal magnet subsystem, and coplanar waveguide with sample.

amplitude, repetition rate, and delay relative to output trigger pulse. Pulse width is adjustable from 100 ps to 10 ns and pulse amplitude is adjustable from 1 mV to 10 V in 1 dB steps. The pulse repetition rate is adjustable from 1 Hz to 100 kHz but is kept fixed at the 100 kHz rate to maximize system throughput. The pulse output is of high quality, with very low jitter [1.5 ps root-mean-square (rms) typical] and high repeatability, and the risetime and pulse shape are independent of width, amplitude, repetition rate, and delay.

To allow measurements of system impulse response, a commercial, passive, impulse-forming network is automatically switched into the path directly following the pulse generator. The impulse-forming network can generate 1 V, 100 ps wide impulses with very repeatable characteristics.

After the 10 V pulse passes through the coplanar waveguide, the response is sent to a computer programmable step attenuator to bring the signal down to a safe level for detection with a digital sampling oscilloscope. The oscilloscope can measure up to a maximum signal of 0.8 V, but a signal level greater than 2 V would damage the high-speed amplifier at the front end. The programmable attenuator is specified for 1 W continuous (100 W peak with maximum pulse width of 10 μ s) operation to 18 GHz and can step from 0 to 81 dB in 1 dB steps. All interconnecting coaxial cables used in the PIMM system are specified for operation to at least 18 GHz.

The 20 GHz digital sampling oscilloscope has up to 15 bits of vertical resolution with averaging, and an unaveraged maximum noise level of less than 0.5 mV rms when operated in its low-bandwidth (12.4 GHz) mode. This specification is essential to the performance of the PIMM due to dynamic range issues inherent in the system. The time interval accuracy is better than 10 ps \pm 0.1% and the timebase resolution can be as fine as 62.5 fs per point. Overall trigger jitter is less than 2.5 ps (timebase and trigger jitter combined). The wave form trace can have up to 4096 data points and up to 4096 trace averages can be specified. The oscilloscope has full computer control over all front panel functions. External attenuator settings can be entered to automatically correct the input voltage and offset range. All of these features allow the system to be fully automated.

Two orthogonal Helmholtz pairs apply static magnetic fields to the sample. These field sources are fully computerized and produce longitudinal bias fields of \pm 12.8 kA/m (160 Oe) and transverse saturating fields of \pm 8.8 kA/m (110 Oe) with a resolution of 0.4 A/m (0.005 Oe). The longitudinal bias field is applied parallel to the waveguide and the transverse saturating field is applied parallel to the field pulses originating in the waveguide, as seen in Figs. 1 and 2. Current is supplied to the magnets via two 10 V, 10 A current calibrators with 0.01% accuracy controlled by a two-channel, 16-bit digital-to-analog converter. The inner magnet has a 10.2 cm (4 in.) bore which allows for easy access to the coplanar waveguide, sample, and interconnecting cables. The field variation across a thin, 1 cm square sample is specified to be less than 1%. Such field uniformity virtually eliminates the possibility of inhomogeneous field effects such as line broadening during a measurement. A photograph of the magnet/waveguide assembly is shown in Fig. 3.



FIG. 3. Closeup of Helmholtz pair showing 10 cm bore revealing coplanar waveguide and high-bandwidth interconnecting cables.

The control software for the PIMM system coordinates all the measurement processes and facilitates rapid data acquisition for each sample. In addition, failsafe measures can be implemented in the measurement algorithms to reduce the chances of damage to the highly sensitive sampling oscilloscope. A screen capture of the front-end panel is shown in Fig. 4. The top section of the panel has various controls and pull-down menus for loading and saving data, setting system parameters and viewing system status, and replaying acquired data sequences. The upper left graph [Fig. 4(a)] shows the raw, unprocessed data consisting of two 10 V pulse traces, one acquired with the sample in a saturated state, and the other acquired in an active state, containing the inductive signals from the sample. The signal from the sample is typically on the order of tens of millivolts in amplitude; thus, the two traces appear to be nearly identical. The two traces must be subtracted in order to extract the inductive signal.

Given that the pulse generator produces 10 V, 55 ps rise-time pulses, it follows that the voltage slew rate is extremely large (over 100 GV/s). This can lead to errors in the subtraction process when two otherwise identical pulses have a small time difference between them. Calculations show that a time difference as small as 100 fs can lead to voltage errors of tens of millivolts, which is often the same size as the signals being measured. The system jitter specifications, while very low, will always lead to time shifts of this magnitude and the result of subtraction is invariably a 10 mV spike at the beginning of the subtracted results. In order to correct for this error, we use a spline fit and interpolation to create two continuous functions that represent the two pulse datasets accurately. The two functions are correlated with each other and the time shift resulting in maximum correlation is used to correct and generate the final subtracted results. These results are corrected for gain and offset variations as well. The middle left-hand side graph [Fig. 4(b)] in Fig. 4 shows these processed and subtracted data.

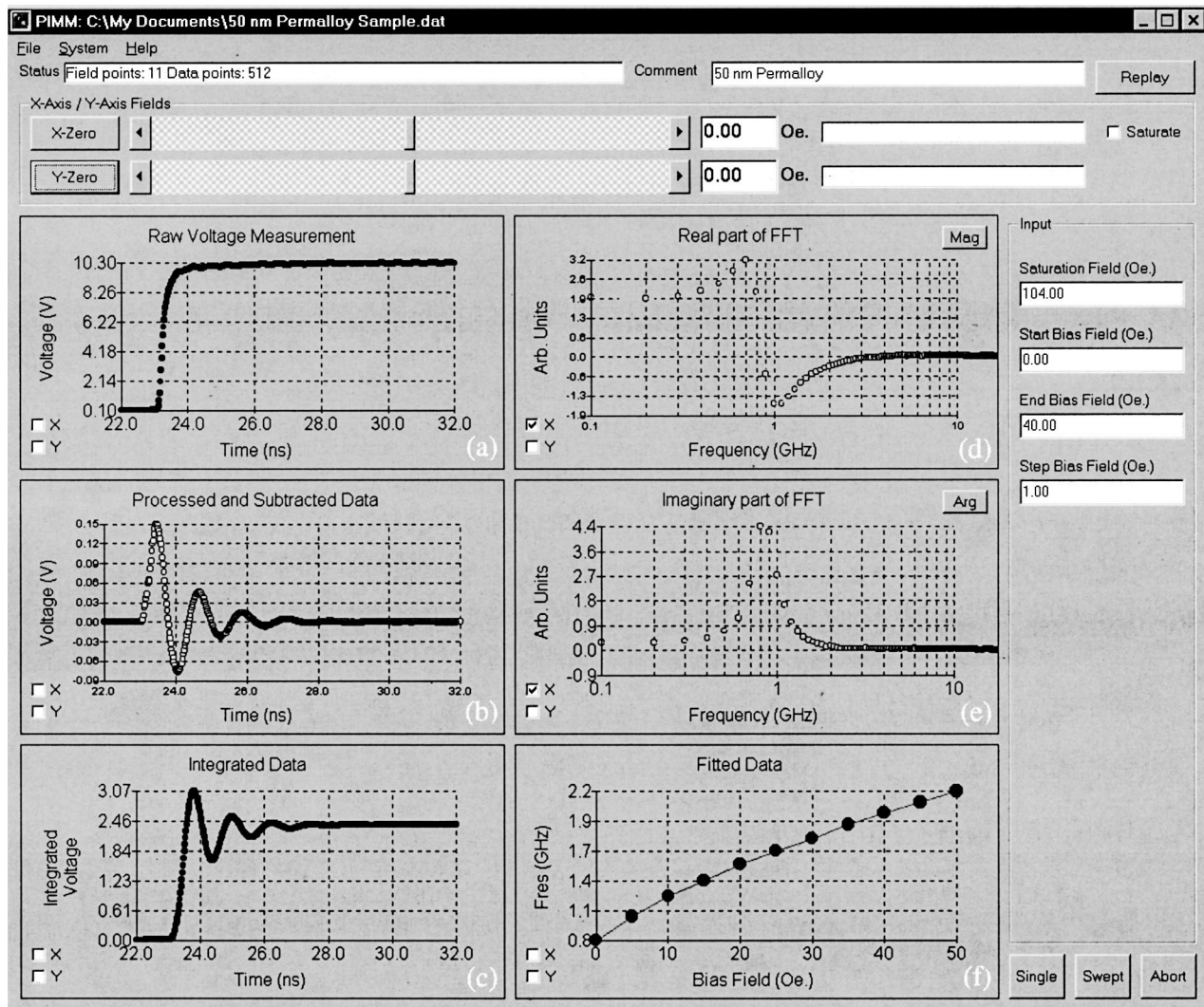


FIG. 4. Screen capture of control program measurement panel. Magnet controls, system status, and pull-down menus are seen at the top. Traces of raw data pulses (a), processed and subtracted inductive data (b), integrated data representing sample magnetization (c), precessional frequency vs longitudinal bias field (f), and imaginary (e) and real (d) part of permeability spectrum can be seen moving clockwise from upper left-hand side.

The graph located in the lower left-hand side corner [Fig. 4(c)] of the system panel shows the results of numerically integrating the processed and subtracted data. This graph illustrates the dynamic response of the magnetization of the sample film. A typical Ni-Fe response is shown with an overshoot and underdamped oscillatory ringing. The oscillations are the result of gyromagnetic spin precession.⁴

The upper [Fig. 4(d)] and middle right-hand side [Fig. 4(e)] graphs show the real and imaginary parts, respectively, of the permeability spectrum as computed from the Fourier transform of the subtracted data shown in Fig. 4(b). These results have been previously shown to be in good agreement with conventional swept-frequency permeability measurements while providing a much greater bandwidth.⁵

The final graph in the lower right-hand side corner [Fig. 4(f)] shows the measured resonance frequency from the permeability spectrum plotted as a function of applied bias field. The precessional frequencies are calculated by zero padding the time data to give higher frequency resolution and then applying a simple linear interpolation to find the zero-crossing point in the real permeability spectrum.

IV. EXPERIMENT

The sample film is placed with the magnetic surface face down onto the clean coplanar waveguide and oriented as desired for a particular measurement. To obtain the greatest sensitivity in the measurement, the sample needs to be as close to the waveguide as possible, without shorting to it. This is achieved by spinning a thin layer of photoresist onto the surface of the sample, or alternatively, a thin piece of tape can be applied to the waveguide. If necessary, a small, nonmagnetic weight is used to hold the sample firmly against the waveguide surface.

Next, the bias field step size and range, saturation field magnitude and direction, pulse amplitude and width, and other system parameters such as number of data points and number of trace averages are entered or default values are accepted. When all the measurement and system parameters have been chosen, the system is ready to proceed. A single measurement or a bias-field swept measurement may be selected. If a single measurement is chosen, the program initiates a sampling oscilloscope acquisition at the current bias

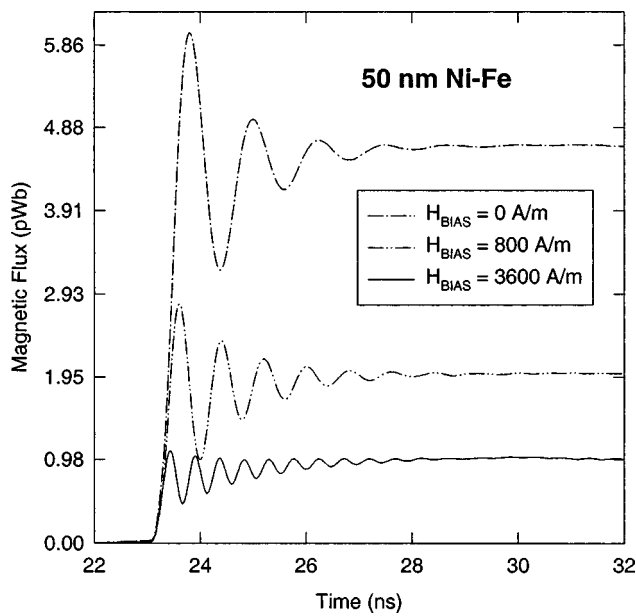


FIG. 5. 50 nm Ni-Fe sample measured at three longitudinal bias fields. The precessional frequency is increased while the signal magnitude is reduced due to the stiffening of the magnetization of the sample with increasing sample bias.

field set by the user. When the required number of trace averages has been acquired, the complete bias-field wave form is downloaded to the computer. The bias field is then set to zero; the saturation field is set to a predefined value, usually close to the maximum of 8.8 kA/m (110 Oe), and another oscilloscope acquisition is initiated. When the required number of averages is completed, the saturated wave form is downloaded to the computer.

For a swept bias-field measurement, the next bias field is applied and the measurement proceeds until all bias fields have been completed. Note that in the aforementioned sequence, the pulse generator is constantly delivering pulses at 100 kHz to the waveguide. For a pulse amplitude of 10 V and a sample in close proximity to the 500 μ m waveguide center conductor, the calculated magnetic field strength due to the pulse current is about 200 A/m (2.5 Oe).⁴ Using waveguides with narrower center conductors increases this value, but at the expense of increased shape anisotropy effects.⁴

V. RESULTS

Figure 5 shows a time trace of the processed, subtracted, and integrated voltage from a 50 nm Ni-Fe film measured at three different longitudinal bias fields. The voltage is integrated to give the magnetic flux, which is proportional to sample magnetization. The flux is strongly affected by the bias field and shows a marked decrease in signal amplitude as the magnetization is stiffened by the bias field, accompanied by a corresponding increase in precessional frequency. Figure 6 shows a plot of squared precessional frequency as a function of longitudinal bias field. The data fall along a straight line, indicating that the precessional frequency is

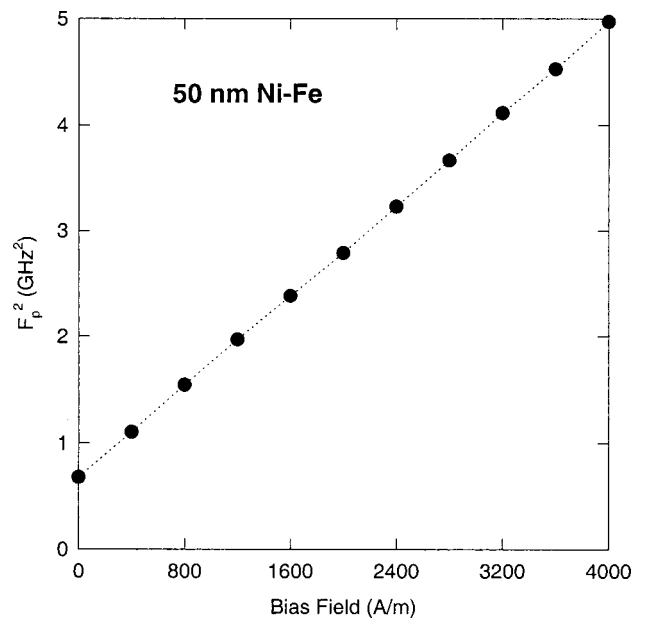


FIG. 6. Squared precessional frequency of 50 nm Ni-Fe sample measured as a function of longitudinal field bias. The straight line indicates agreement with standard FMR calculations.

proportional to the square root of the bias field, as predicted by ferromagnetic resonance (FMR) theory for fields parallel to the sample plane.¹³

Three time traces showing the magnetic response of Tb-doped Ni-Fe samples as a function of Tb concentration are shown in Fig. 7. The curves have been displaced so that they may be seen together. The top trace, containing no Tb, appears identical to the top trace in Fig. 5 and shows a typical underdamped Ni-Fe response. The middle trace of Fig. 7 shows a Ni-Fe sample doped with 2% Tb. This response is an almost perfect example of critical damping, with only a slight overshoot. The bottom trace shows a response that is

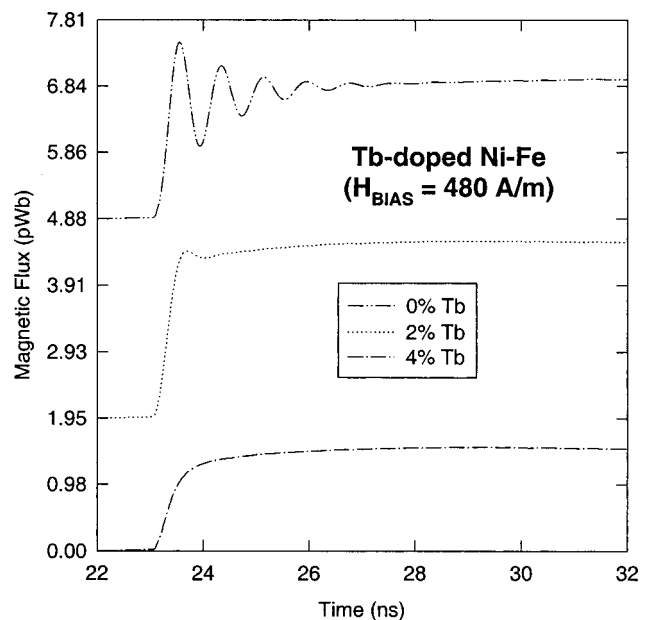


FIG. 7. Magnetodynamics of Tb-doped Ni-Fe samples as a function of Tb-doping percentage. The sample response is progressively damped as the Tb content is increased.

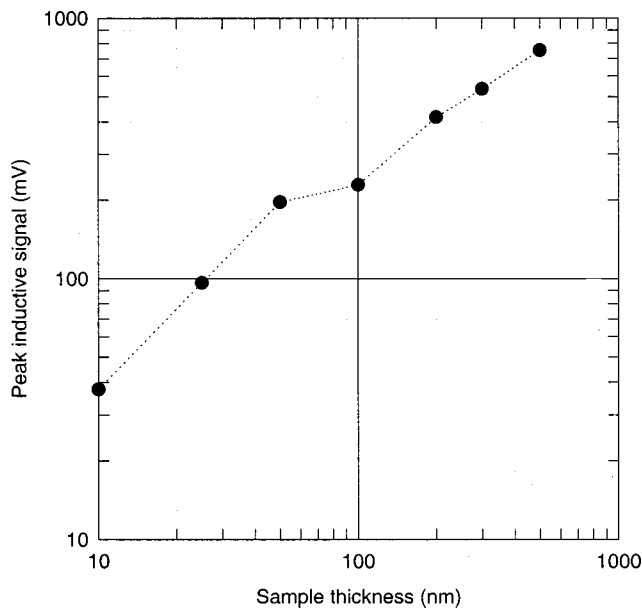


FIG. 8. Peak amplitude of induced magnetic signal as a function of Ni-Fe film thickness. The trend is mostly linear, but two regimes appear to be present.

significantly overdamped, as a result of 4% Tb doping. This response is the weakest signal with the slowest risetime, yet the signal is easily and repeatably measured.

To estimate the sensitivity of the PIMM system using the existing coplanar waveguide, we measured a series of Ni-Fe films of varying film thickness but constant surface area. The longitudinal bias field was zero for these measurements. The peak value of the induced signal, as seen in Fig. 4(b), was measured as a function of film thickness. These data are plotted in Fig. 8. As shown in Fig. 8, the data mostly follow a linear dependence of signal strength on film thickness, although there appear to be two sensitivity regimes.

VI. DISCUSSION

The sensitivity of the instrument, as determined from the data shown in Fig. 8, indicates that the current version of the PIMM can measure films with areas of 18 mm \times 18 mm that are as thin as 2 nm. This is computed by assuming a signal-to-noise ratio of 20, an oscilloscope raw noise level of about 16 μ V rms with 4096 signal averages,⁴ an input attenuation of 23 dB (required for 10 V pulses), and then extrapolating linearly from the data shown in Fig. 8. The raw oscilloscope noise level looking into the attenuator is then approximately 226 μ V rms, implying that the induced signal must be roughly 4.5 mV in magnitude to be adequately measured. Extrapolating the data in Fig. 8 to this level yields the aforementioned value for minimum film thickness.

Improvements to the sensitivity of the PIMM would allow an even greater variety of film samples to be measured. A serious constraint upon sensitivity is the large dynamic range required to accept 10 V pulses, while still measuring inductive signals in the range of tens of millivolts. To improve the sensitivity a differential detection scheme that uses an analog mixer on the front end of the sampling oscilloscope could be implemented. Such an approach would

greatly reduce the amplitude of the signal entering the oscilloscope and thus increase the dynamic range and sensitivity of the measurement. If the attenuation were reduced to zero on the front end of the sampling oscilloscope and all other factors remained the same, the minimum measurable film thickness, calculated previously, would be reduced by more than an order of magnitude. In addition, an improvement in the overall system bandwidth, limited partly by the quality of the coplanar waveguide, could be easily achieved by improved waveguide construction.

The repeatability of the instrument is quite good (better than 5%) when reasonable care is taken to make sure that the sample film lies flat on the surface of the waveguide. Minor differences in film spacing, due to dust particles, appear as variations in pulsed field and induced signal strength. Field variations typically are not significant and continue to remain in the small signal (small rotation angle) regime. Signal strength variations due to sample spacing, which are still within the sensitivity of the instrument, are designed to be removed by the background subtraction process applied to the saturated magnetic film.

In order to accurately assess the time and frequency performance of the coplanar waveguide, it is necessary to characterize its bandwidth. The step risetime used to determine the bandwidth originates from a 35 ps (as measured using the sampling oscilloscope) time-domain-reflectometry step generator. The risetime of this step, transmitted through the empty coplanar waveguide, and measured using the sampling oscilloscope is 49 ps. The risetime of the waveguide is then $(49^2 - 35^2)^{1/2} = 34.3$ ps, which corresponds to a transmitted bandwidth of more than 10 GHz. The overall system bandwidth, measured in the same manner, is approximately 6 GHz. Using this system bandwidth and standard FMR theory,¹³ we would predict a maximum measurable anisotropy field of about 3.2 kA/m (400 Oe).

When a conductive sample is placed onto the waveguide, eddy current losses lead to a broadening of the step risetime. This broadening, which corresponds to a loss of bandwidth, is detrimental to the performance of the waveguide and will appear as increased damping in a given measured response. The eddy current loss can arise in two ways: (1) the sample itself can be thick enough and conductive enough to affect the bandwidth, and (2) the sample substrate, usually much thicker, can have a smaller, yet still significant conductivity, enough to affect the generated field over its volume. This is why glass substrates need to be used to make the magnetic films to be measured. Si substrates, especially those with *n*- or *p*-type doping, can have excessive conductivity.

We have measured Ni-Fe films below thicknesses of 200 nm and have found that this is roughly the crossover threshold into the eddy current regime (for films deposited onto glass cover slides 18 mm \times 18 mm in size). Films above 200 nm have a noticeable damping, as indicated by a reduction of the precessional effects normally seen in Ni-Fe samples. In addition, these samples begin to widen the transmitted risetime of the applied field pulse. At sample thickness of 400 and 500 nm, eddy current effects are dominant—there is no precessional ringing at all and the bandwidth of

the system is reduced to below 1 GHz, as seen by a marked increase in the step risetime transmitted through the waveguide.

The permeability spectrum is calculated directly from the FFT of the induced signal voltage seen in Fig. 4(b). This is contrary to the normal definition of permeability, which requires division by the exciting field to extract permeability. We have found that our step generator produces steps ideal enough to allow linear system theory to be applied to simplify the calculation. The idealized step function essentially corresponds, in the frequency domain, to dividing the FFT of the induced voltage by a constant—hence, the permeability spectrum is computed from these data alone, since calibration of the data already requires multiplication by a constant. Also, in order to remove the frequency domain effects of the variable time shift apparent in the time trace of induced voltage (the data has a variable leading edge before the step transition occurs that can not be fixed) we must compensate for the arbitrary rotation $e^{ik\tau}$ where τ is the arbitrary time shift. This is accomplished by rotating the real and imaginary parts of the complex permeability spectrum until the imaginary part is zero, as expected, at low frequencies.

The PIMM can yield calibrated results if a sample of standard geometry and surface area, calibrated with a vibrating sample magnetometer or other calibration technique, is compared with another sample of the same geometry and surface area. Measurements designed to give the ratio of saturation magnetization or permeability for two unknown samples are also possible. An important assumption here is that we are far from the threshold of the eddy current regime; otherwise, two samples of different thickness can give essentially the same results.

The PIMM system completes measurements very quickly and easily and with a high bandwidth. Improving the

coplanar waveguide, which is by no means optimized, can easily increase the bandwidth of the system. The coplanar waveguide and sample can also be incorporated onto a single lithographed wafer and measured using high-bandwidth microwave probes. This would allow measurement of a precise sample geometry with narrow waveguide spacings (necessary to produce larger pulsed fields), and permit the study of other sample geometries. The PIMM can measure FMR frequencies, high-frequency damping, dynamical anisotropy, and other useful magnetic properties⁴ on samples at the coupon level. It can measure magnetic properties as a function of sample thickness, composition, and orientation. PIMM is a robust and flexible measurement technique that permits rapid evaluation of thin-film materials for data storage and rf applications.

¹K. B. Klaassen, R. G. Hirko, and J. T. Contreras, *IEEE Trans. Magn.* **34**, 1822 (1998).

²Western Digital Caviar 30 GByte per platter, press release, Feb. 26, 2001.

³IBM Ultrastar 73 LZX specifications, 697 Mbps media transfer rate.

⁴T. J. Silva, C. S. Lee, T. M. Crawford, and C. T. Rogers, *J. Appl. Phys.* **85**, 7849 (1999).

⁵C. Alexander, J. Rantschler, T. J. Silva, and P. Kabos, *J. Appl. Phys.* **87**, 6633 (2000).

⁶D. O. Smith, *J. Appl. Phys.* **29**, 264 (1958).

⁷P. Wolf, *J. Appl. Phys.* **32**, 95S (1961).

⁸W. K. Hiebert, A. Stankiewicz, and M. R. Freeman, *Phys. Rev. Lett.* **79**, 1134 (1997).

⁹M. Bauer, R. Lopusnik, J. Fassbender, and B. Hillebrands, *Appl. Phys. Lett.* **76**, 2758 (2000).

¹⁰W. Bailey, P. Kabos, F. B. Mancoff, and S. E. Russek, *IEEE Trans. Magn.* **37**, 1749 (2001).

¹¹S. E. Russek, P. Kabos, T. J. Silva, F. B. Mancoff, D. X. Wang, Z. H. Qian, and J. M. Daughton, *IEEE Trans. Magn.* **37**, 2248 (2001).

¹²T. M. Crawford, M. Covington, and G. J. Parker, *Proceedings of the 8th Joint MMM-Intermag Conference*, San Antonio, TX, 7–11 January 2001.

¹³C. Kittel, *Introduction to Solid State Physics*, 7th ed. (Wiley, New York, 1996), p. 505.